# Adsorption Performance of SiO₂/CPAM Composites for Aqueous Ca(II)

Shan Li,[a]  Fa Chen,[a] Furong Lin,[a] Yong Kong,[a] and Hongqi Dai [b,*]

Silica/cationic polyacrylamide (SiO₂/CPAM) composites with a dendritic structure were prepared *via in situ* polymerization based on silica containing vinyl groups and acrylamide monomers. The structure and surface properties of the composites were revealed with scanning electron microscopy (SEM), transmission electron microscopy (TEM), Fourier-transformed infrared spectroscopy (FT-IR) and X-ray photoelectron spectroscopy (XPS). The adsorption behavior and properties of aqueous Ca(II) on the SiO₂/CPAM composites were also investigated. The effect of the pH value, the initial Ca(II) concentration, adsorption time, and temperature on adsorption properties were examined. The results showed that the SiO₂/CPAM composites displayed a high adsorption performance for aqueous Ca(II). The maximum adsorption capacity of the SiO₂/CPAM composites for Ca(II) was 123.4 mg•g$^{-1}$ at room temperature and pH 9. The adsorption behavior was in agreement with the Langmuir isotherm model. The adsorption was an endothermic and spontaneous process. Adsorption kinetics fitted well with the pseudo-second-order model. The adsorption of Ca(II) on the SiO₂/CPAM composites was mainly attributed to chemical interaction, and chelation was more significant than electrostatic interaction.

*Contact information: a*: *School of Petrochemical Engineering, Changzhou University, Changzhou, Jiangsu 213164, China; b*: *Jiangsu Province Key Lab of Pulp and Paper Science and Technology, Nanjing Forestry University, Nanjing, Jiangsu 210037, China; *Corresponding author: hgdhq@njfu.edu.cn*

## INTRODUCTION

Calcium ion (Ca(II)) is widely found in natural water bodies. It is involved in the production processes of industry and agriculture, as well as the biological activities of organisms. However, excess calcium ions have many negative consequences. In industrial production, water containing a high content of calcium ions causes incrustation scale, which decreases the heat transfer efficiency of heat exchangers. The accumulation of metal ions such as Ca(II) and Mg(II) in the closed whitewater systems of the papermaking industry has adverse effects, such as disturbing the wet-end chemical balance, affecting operation stability of the paper machine, and decreasing product quality (Gao *et al.* 2009; Ba and Cao 2014; Sun *et al.* 2014). There are many methods for Ca(II) removal from aqueous solutions, such as filtering, ion exchange, adsorption, precipitation, and complexation (Fan *et al.* 2012; Hemalatha *et al.* 2017; Hettiarachchi *et al.* 2017). Among these, complex formation can be regarded as the simplest and most economical method.

It is also an effective method for controlling multivalent metal ions by taking advantage of the "soft-hard-acid-base" theory (Elving *et al.* 1987) to design a polymer that can exert complexation with Ca(II). Ye *et al.* (2009) reported that the modified natural polymer (named as ACS) containing carboxyl groups can control aqueous Ca(II), and the

Ca(II) adsorption amount was 32.0 mg•g$^{-1}$ with a removal of 81%. Sun *et al.* (2012) synthesized an amphoteric polymer (P(AM-DMDAAC-AA)) to regulate Ca(II) with an adsorption amount of 80.2 mg•g$^{-1}$. Chen and Yu (2013) prepared a poly(acrylate-acrylamide) adsorbent resin to adsorb Ca(II) in hard water with a maximum adsorption amount of 108.0 mg•g$^{-1}$. However, the adsorption performance of all known adsorbents is still not satisfactory.

Polyacrylamide (PAM) is a water-soluble polymer with amino ($-NH_2$) groups on the molecular chain. It is an ideal material used for designing and preparing water treatment agents with specific applications through the introduction of various functional monomers, such as for the removal of hazardous materials. Furthermore, it is common for PAM to be combined with inorganic materials in composites to resolve a number of practical problems (Zhao *et al.* 2010; Wang and Li 2015).

Silica ($SiO_2$) or mesoporous silica can be mixed with or bonded to PAM to produce composite adsorbents or hydrogels due to its large specific surface area, high chemical stability, and ease of modification. They can be widely applied for the removal of heavy metal ions or organic substances from aqueous solution, such as lead (Ghorai *et al.* 2012), mercury (Saad *et al.* 2016), cholesterol (Clausen *et al.* 2014), aniline (An *et al.* 2009a), dyestuffs (Hadizade *et al.* 2017), and 2,4,6-trinitrotoluene (TNT) (An *et al.* 2009b). $SiO_2$/PAM composite resin can be synthesized through an *in situ* sol-gel method using tetraethyl orthosilicate (TEOS) in the solution of acrylamide monomers. $SiO_2$/PAM composite adsorbent resin has also been obtained after modification with sulfomethylation for adsorbing metal ions, such as Pb(II) and copper(II) (Li *et al.* 2012). $SiO_2$/PAM composites have numerous possible applications in industrial wastewater treatment.

In this work, dendritic $SiO_2$/cationic polyacrylamide composites ($SiO_2$/CPAM) were fabricated by copolymerization of acrylamide and silica microspheres containing vinyl groups (vinyl-$SiO_2$) for adsorbing the aqueous Ca(II). A number of vinyl groups on the surface of vinyl-$SiO_2$ can be copolymerized with other vinyl monomers to form $SiO_2$-based dendritic composites connected by $SiO_2$ cores. Composites with such structure and components can greatly increase the adsorption for Ca(II). The influence of the pH value, initial Ca(II) concentration, adsorption time, and temperature on the adsorption properties of $SiO_2$/CPAM were systematically investigated. The adsorption kinetics, thermodynamics, and mechanisms of Ca(II) adsorption onto $SiO_2$/CPAM were also discussed.

## EXPERIMENTAL

### Reagents and Materials

Acrylamide (AM), anhydrous ethanol, potassium persulfate ($K_2S_2O_8$), sodium hydrogen sulfite ($NaHSO_3$), ethylene diamine tetraacetic acid disodium salt (EDTA•2Na), hydrogen chloride (36.0-38.0 wt.%), chrome black T, calcium chloride, ammonium chloride, and ammonium hydroxide (25.0-28.0 wt.%) were obtained from Sinopharm Chemical Reagent Co. (Shanghai, China). 2,2-Azobis (2-methylpropionamidine dihydrochloride) (AIBA•2HCl) was purchased from Sigma-Aldrich (St. Louis, USA). Vinyltriethoxysilane (VTES) was obtained from Energy Chemical (Shanghai, China). Acryloyloxyethyl trimethyl ammonium chloride (DAC, 85.5 wt.%) was supplied by Shandong Liyuan Guosheng Chemical Co. (Jinan, China). All chemicals were used without further purification. Ultrapure water (18.2 MΩ•cm) was used directly from a Milli-Q water system. Filtering film (50 mm/0.45 μm) was provided by Shanghai Xinya Purification

Equipment Co. (Shanghai, China).

## Preparation of SiO₂/CPAM Composites

*Preparation of vinyl-SiO₂*

Vinyl-SiO₂ was prepared as described (Deng *et al.* 2009) with minor modifications. In brief, 3 mL of VTES was dispersed in 50 mL of water under vigorous magnetic stirring (300 rpm), which was followed by addition of 0.05 mL of 2 M HCl aqueous solution. The mixture was stirred for a certain time until a transparent solution was obtained. Next, 0.6 mL of ammonium hydroxide was added dropwise into the reaction mixture, and the reaction proceeded at room temperature for 2 h. The final mixture contained 5.08 wt.% VTES and 0.26 wt.% $NH_3•H_2O$. After completion of the reaction, the reaction mixture was centrifuged at 2,000 rpm for 10 min, which was followed by ultrasonic treatment in ethanol to remove impurities such as ammonia, water, and unreacted VTES. The same separation process was repeated thrice. Finally, the resulting particles were dried at room temperature.

*Preparation of SiO₂/CPAM composites*

Vinyl-SiO₂ was adopted as the substrate for *in situ* copolymerization of AM and DAC. In a typical process, 0.0391 g of dry vinyl-SiO₂, 2.2808 g of AM (1/3 of the total mass), and 1.1427 g of DAC were mixed in water. The mixture was sonicated for 5 to 10 min and then added to a four-necked flask equipped with a condenser and mechanical agitation. To prevent oxygen during the synthesis, a flow of nitrogen gas was introduced into the mixture for 30 min. Next, 0.0015 g of EDTA and 0.0047 g of $NaHSO_3$ were added into the flask. The remaining 2/3 AM and the initiator solution containing $K_2S_2O_8$ and AIBA•2HCl (0.6 wt.% based on total monomer mass, in which AIBA•2HCl was 35.0 wt.%) were dropped slowly into the mixture at 40 °C. The temperature was controlled using a thermostat water bath. The mixture was reacted at this temperature for 2 h and then 65 °C for another 4 h; a transparent yellow solution was obtained. The crude composites were precipitated with ethanol, washed with ethanol several times, and dried at room temperature.

## Characterization

Scanning electron microscopy (SEM) images were recorded using a JEOL JSM-6360LA microscope (Tokyo, Japan). Transmission electron microscopy (TEM) was performed on a JEOL JEM-2100 microscope operating at an accelerating voltage of 200 kV. Fourier transform infrared (FT-IR) spectra of different samples were measured on a Shimadzu Nicolet FTIR-8400S spectrophotometer (Kyoto, Japan) using KBr pellets. X-ray photoelectron spectroscopy (XPS) studies were performed with a VG Corporation ESCALAB MKII spectrometer (London, UK) with an Al Kα X-ray source.

## Batch Adsorption Studies

The adsorption ability of SiO₂/CPAM was measured by titration. In a typical process, 0.08 g of dry SiO₂/CPAM sample was dissolved with ultrapure water and then transferred into a 100 mL volumetric flask, where $CaCl_2$ ($V_0$, $c_1$:0.1 mol•L$^{-1}$) was added. The volume of the flask was metered with ultrapure water, followed intermittent oscillation at room temperature. After 90 min, the solution was filtered with the filtering film, and 10 mL of the supernatant was placed in a 250 mL Erlenmeyer flask with 10 mL of $NH_3$-$NH_4Cl$ buffer solution (pH = 10) and 50 mg of chrome black T solid indicator. The mixture was titrated with EDTA standard solution ($c_2$: 0.002 mol•L$^{-1}$) so that the endpoint would be

indicated by the change of the mixture hue from wine-red to blue. The result was the average value of three measurements.

The adsorption capability of $SiO_2/CPAM$ for Ca(II) was calculated by Eq. 1,

$$Q = \frac{V_0 c_1 - 10 c_2 V}{m} \tag{1}$$

where $Q$ (mmol•g$^{-1}$) is the adsorption capability of $SiO_2/CPAM$ for Ca(II), $m$ (g) is the mass of samples, $c_1$ (mol•L$^{-1}$) and $c_2$ (mol•L$^{-1}$) are the concentrations of $CaCl_2$ and EDTA, respectively, and $V_0$ (mL) and $V$ (mL) are the consumed volumes of $CaCl_2$ solution and EDTA standard solution at the endpoint, respectively. The adsorption ability was also expressed as $Q_m$ (mg•g$^{-1}$, $Q_m = 40.078Q$), in order to compare the results with data from the literature.

The residual Ca(II) concentration was calculated by Eq. 2,

$$c_r = \frac{1000 c_2 V}{V'} \tag{2}$$

where $c_r$ (mol•L$^{-1}$) is the residual Ca(II) concentration in the sample solution and $V'$ (mL) is the total volume of the sample solution.

## RESULTS AND DISCUSSION

### Characterization of SiO₂/CPAM Composites

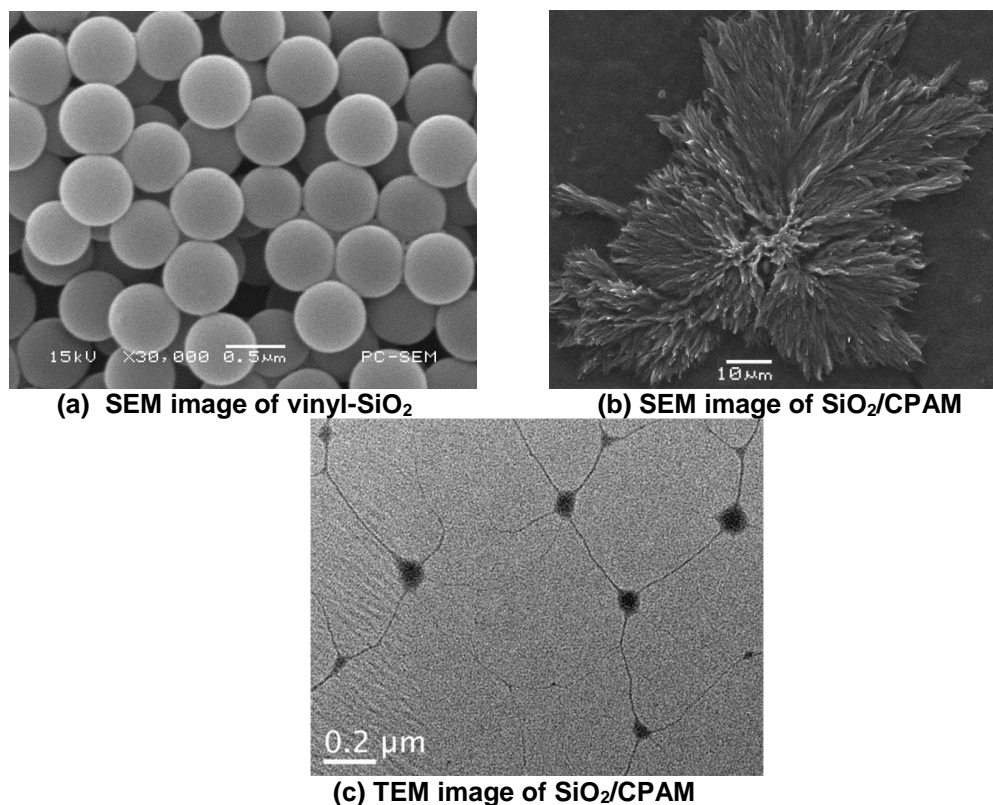Figure 1a shows the SEM image of vinyl-$SiO_2$.



**(a) SEM image of vinyl-SiO₂**      **(b) SEM image of SiO₂/CPAM**

**(c) TEM image of SiO₂/CPAM**

**Fig. 1.** SEM images of vinly-SiO₂ (a) and SiO₂/CPAM (b), and TEM of SiO₂/CPAM (c)

*bioresources*.com

The microparticles were complete spheres with a uniform dispersion and smooth surface, and they had an average diameter of approximately 625 nm. Figure 1b displays the SEM image of $SiO_2$/CPAM. The micromorphology of the composites presented a distinct dendritic structure with a center of vinyl-$SiO_2$. Also, it was demonstrated more clearly that the composites were connected by the vinyl-$SiO_2$ microparticles from Fig. 1c, because vinyl groups on the surface of vinyl-$SiO_2$ can make them copolymerized with AM and DAC *via in situ* polymerization. They linked the organic molecular chains together to form a large dendritic structure.

The IR spectra of vinyl-$SiO_2$ and $SiO_2$/CPAM are shown in Fig. 2. The peaks at 3352 $cm^{-1}$ and 3194 $cm^{-1}$ were ascribed to asymmetrical and symmetrical stretching vibrations of N–H in primary amide groups (Li *et al.* 2006; Pirzada *et al.* 2012, 2014; Pan 2015); these peaks overlapped with the 3400 to 3500 $cm^{-1}$ band of $\equiv$Si–O–H in the $SiO_2$/CPAM composites. The peak at 3025 $cm^{-1}$ corresponded to =CH stretching vibrations in vinyl-$SiO_2$ spheres, which was not seen in the $SiO_2$/CPAM composites. However, new distinct –$CH_3$ and –$CH_2$ peaks were found in the $SiO_2$/CPAM composites at 2940 $cm^{-1}$ and 2866 $cm^{-1}$, respectively. The strong absorbing peak at 1662 $cm^{-1}$ corresponded to C=O stretching vibrations, while peaks at 1611 $cm^{-1}$ and 1451 $cm^{-1}$ corresponded to N–H bending vibrations and –$CH_2$ bending vibrations in –$CH_2$–$N^+(CH_3)_3$, respectively. Peaks at 1128 $cm^{-1}$ and 1045 $cm^{-1}$ were attributed to Si–O–Si stretching vibrations in vinyl-$SiO_2$. A Si–C stretching vibration band appeared at 767 $cm^{-1}$. These peaks confirmed the presence of vinyl-$SiO_2$, and they were connected to AM and DAC *via in situ* copolymerization to form a dendritic structure.
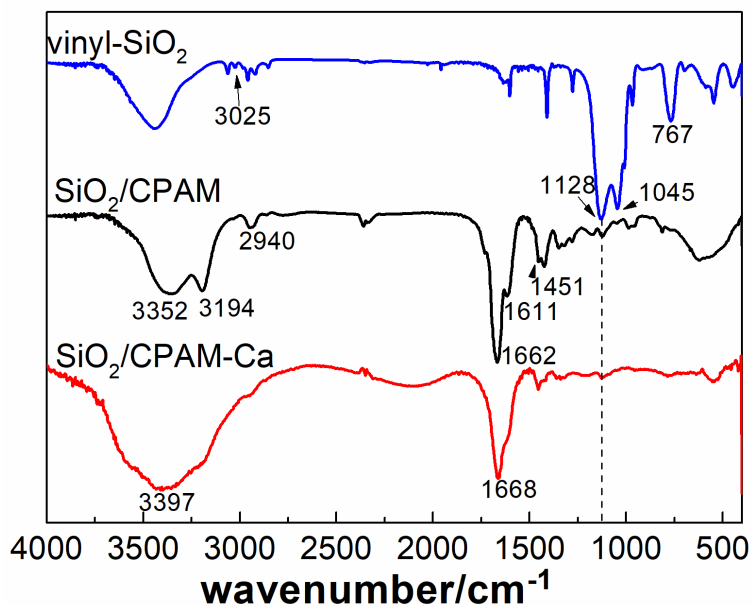


**Fig. 2.** IR spectra of vinyl-$SiO_2$, $SiO_2$/CPAM, and $SiO_2$/CPAM-Ca

The typical sampling depth by using XPS was 2 to 10 nm so that the surface elemental compositions of the particles could be obtained for the near surface. Figure 3 demonstrates the XPS survey spectra recorded for the $SiO_2$/CPAM composites. Carbon, oxygen, silicon, nitrogen, and chlorine were detected by XPS on the surface of $SiO_2$/CPAM.

Figure 3a shows Si 2p and Si 2s signals at 101.9 eV and 152.5 eV, respectively, indicating the presence of silica at the surface of the $SiO_2$/CPAM composites (Fielding *et al.* 2011). The peaks at 101.6 eV, 102.0 eV, and 102.6 eV from Fig. 3c were attributed to $Si(-O)_1$, $Si(-O)_2$, and $Si(-O)_3$, respectively (Alexander *et al.* 1999), confirming the existence of hybrid silica without $Si(-O)_4$. Deconvolution of the XPS for C 1s electron of $SiO_2$/CPAM (Fig. 3b) presents carbon in three different chemical states. The dominant component at 284.7 eV was related to the C atom of C–C linkage, and the resolved weak component at 286.5 eV was attributed to C–O linkage (Jedlicka *et al.* 2007; Peng *et al.* 2014). However, the peak at 288.0 eV corresponded to C=O bonding of N–C=O (Jedlicka *et al.* 2007). Thus, AM residues appeared mainly on the surface of $SiO_2$/CPAM, and the C–O bonding was attributed to DAC or VTES residue ($CH_2CH_3$–O–Si≡) that was not hydrolyzed completely. It was concluded that vinyl-$SiO_2$ was preferentially reacted with the positively charged DAC and then copolymerized with AM. The positive charges within the polymer chains made the dendritic structure of $SiO_2$/CPAM well-dispersed in solution, reducing the aggregates and leading to excellent adsorption behavior.
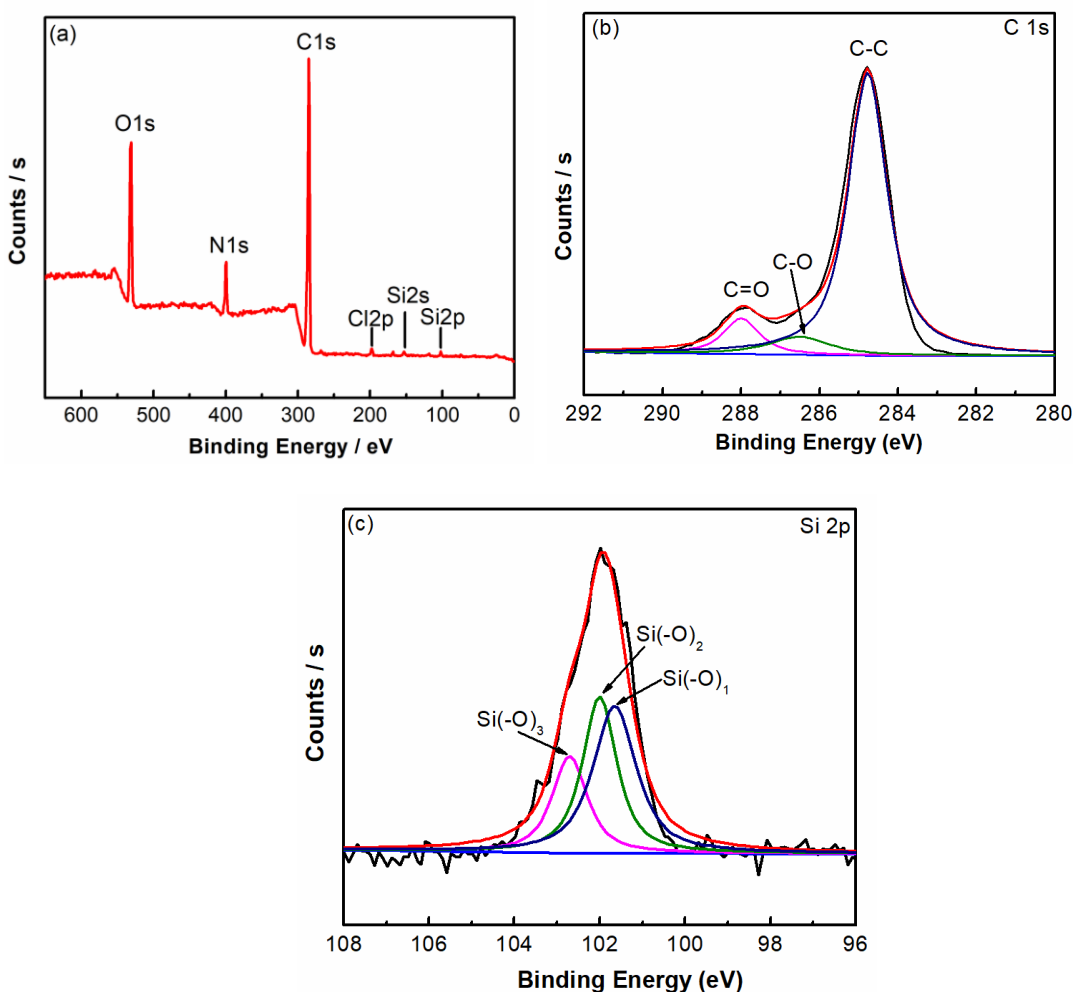


**Fig. 3.** XPS survey spectra recorded for $SiO_2$/CPAM (a) and C 1s (b), and Si 2p (c) XPS spectra

## Effects of the pH Value and Initial Ca(II) Concentration

The pH value was closely related to the presence of Ca(II) in the solution. To investigate the effect of pH, the sorption experiments were conducted with an initial Ca(II) concentration of 5.0 mmol•L$^{-1}$, as shown in Fig. 4. The Ca(II) adsorption amount ($Q$) increased with the pH value, while the residual Ca(II) concentration decreased continuously. The excess H$^+$ had a competitive adsorption with the positively charged Ca(II) in the lower pH values (1 to 3), resulting in a decreased adsorption of Ca(II) in the active sites of SiO$_2$/CPAM. In addition, the surface of the silica spheres and the functional groups on the polymer chain were protonated to form $\equiv$Si−OH, $\equiv$Si−OH$_2^+$, or −NH$_3^+$ so that electrostatic repulsion occurred between the metal ions and the protonated polymers (Kong *et al.* 2011), leading to the decline of the adsorption ability. The adsorption increased abruptly at pH 12 due to the formation of CaCO$_3$ precipitation in the strong alkaline condition (Sun *et al.* 2012). When the pH value was in the range of 8 to 11, $Q$ had a maximum value and the adsorption was close to saturation.
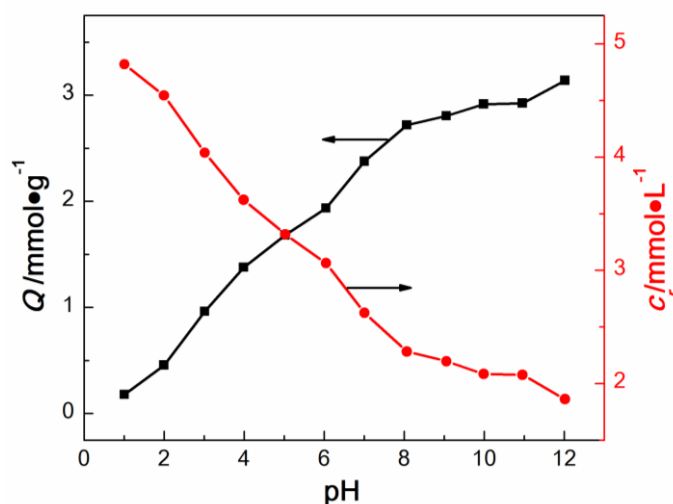


**Fig. 4.** Effect of the pH value on the adsorption amount and residual Ca(II) concentration

The effect of the initial Ca(II) concentration was investigated while maintaining a pH value of 9, as demonstrated in Fig. 5. When the initial Ca(II) concentration was varied from 1.0 to 9.0 mmol•L$^{-1}$, the adsorption amount increased rapidly, indicating the active sites on SiO$_2$/CPAM were available. A possible reason was that increasing the concentration of metal ions can increase the effective collision odds between metal ions and adsorbents, leading to the increase of the adsorption amount (Wu *et al.* 2012). The residual Ca(II) concentration also increased with increment of the initial Ca(II) concentration. When the initial Ca(II) concentration was less than 9 mmol•L$^{-1}$, the residual Ca(II) concentration increased slightly, indicating an unsaturated adsorption process. When the initial Ca(II) concentration was more than 9 mmol•L$^{-1}$, the adsorption amount increased continuously until it leveled off at 13 mmol•L$^{-1}$, while the residual Ca(II) concentration also grew greatly. This result can be interpreted as the adsorption sites gradually becoming saturated and the electrostatic repulsion and steric hindrance both hindering the further adsorption of SiO$_2$/CPAM for Ca(II) gradually. Therefore, the optimal initial Ca(II) concentration was 13 mmol•L$^{-1}$.
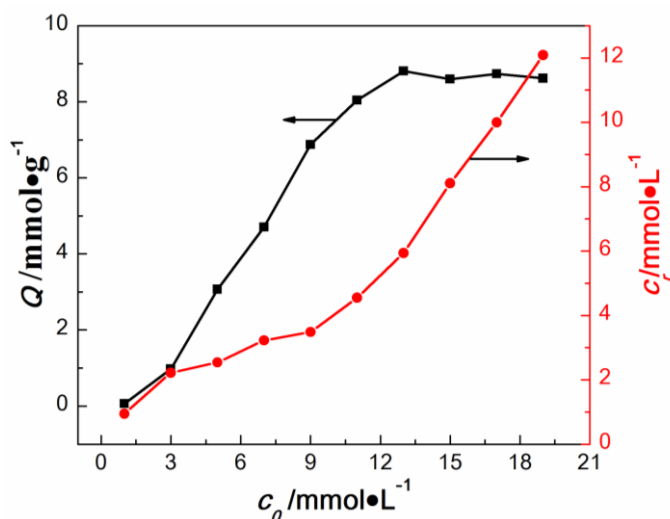
**Fig. 5**. Effect of the initial Ca(II) concentration on the adsorption amount and residual Ca(II) concentration
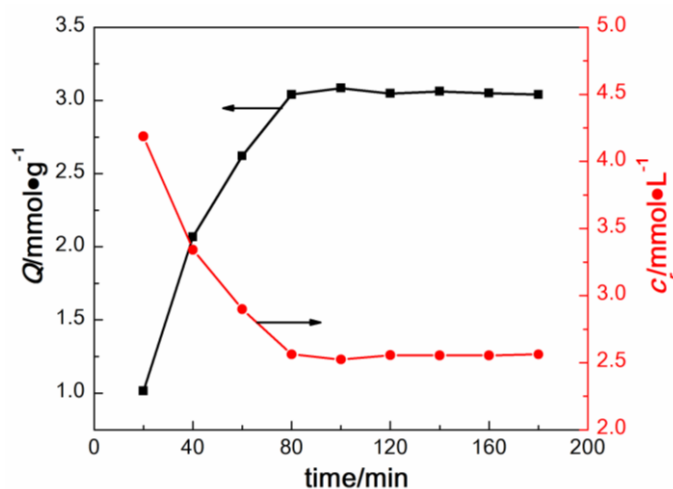


**Fig. 6.** Effect of the adsorption time on the adsorption amount and residual Ca(II) concentration

## Adsorption Kinetics

The effect of the adsorption time (in the range of 20 to 180 min) was investigated while maintaining a pH value of 9 and an initial Ca(II) concentration of 5.0 mmol•L$^{-1}$, as shown in Fig. 6. At the beginning, the adsorption amount increased with the adsorption time; it then reached a platform with a maximum amount of 3.08 mmol•g$^{-1}$. In other words, SiO$_2$/CPAM can adsorb 123.4 mg Ca(II) per gram when the adsorption time was equal to or more than 80 min. At the same time, the adsorption process reached equilibrium and the residual Ca(II) concentration remained constant.

To further determine the adsorption kinetics of Ca(II) on the SiO$_2$/CPAM composites, the obtained data in Fig. 6 were fitted with the pseudo-first-order kinetic model (Eq. 3) and the pseudo-second-order kinetic model (Eq. 4) (Azizian 2004; Li *et al.* 2015; Mohanta and Ahmaruzzman 2018),
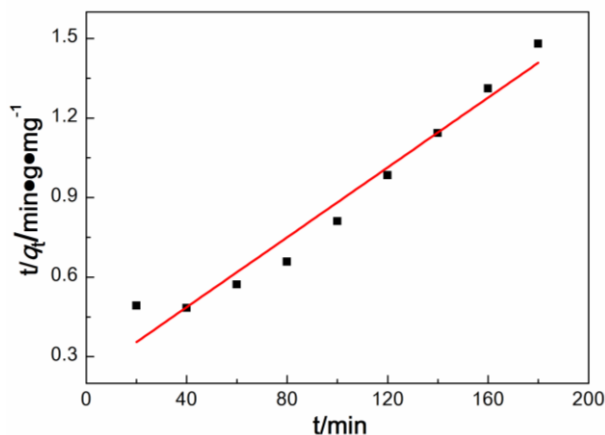
$$\ln (q_e - q_t) = \ln q_e - k_1 t \tag{3}$$

$$\frac{t}{q_t} = \frac{1}{k_2 q_e^2} + \frac{t}{q_e}$$

(4)

where $q_e$ (mg•g$^{-1}$) and $q_t$ (mg•g$^{-1}$) are the amounts of Ca(II) adsorbed at equilibrium and at time $t$ (min), respectively, and $k_1$ (min$^{-1}$) and $k_2$ (g•mg$^{-1}$•min$^{-1}$) are the pseudo-first-order and pseudo-second-order rate constants, respectively.
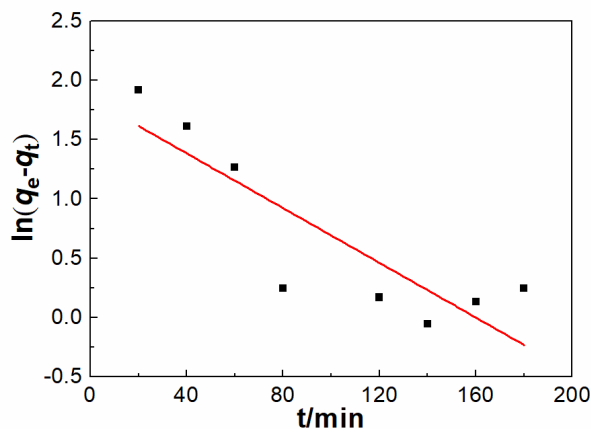


**(a) Pseudo-first-order model linear fitting**



**(b) Pseudo-second-order model linear fitting**

**Fig. 7.** Pseudo-first-order model linear fitting and pseudo-second-order model linear fitting

The plots of ln($q_e$-$q_t$) *versus* $t$ and $t/q_t$ *versus* $t$ are shown in Fig. 7. The dynamic parameters and correlation coefficients were calculated by the fitting equations and are shown in Table 1. The $R^2$ (0.9559) corresponding to the plot fitted with the pseudo-second-order kinetic model was higher than that obtained from the pseudo-first-order kinetic model (0.7163), and the calculated equilibrium adsorption amount ($q_e$=123.4 mg•g$^{-1}$) was essentially the same as the experimental value (123.4 mg•g$^{-1}$), indicating that the adsorption kinetics of SiO$_2$/CPAM for Ca(II) can be better described by the pseudo-second-order model. Furthermore, the formation of chemical bonds was the main factor affecting the pseudo-second-order adsorption, which also illustrated that the adsorption process was mainly chemisorption (Bai *et al.* 2011).

**Table 1.** Kinematic Models' Linear Regressions and Kinetics Parameters of Adsorption of $SiO_2$/CPAM for Ca(II)

| Kinetic Model | Kinetic Parameters | $R^2$ |
|---|---|---|
| Pseudo-first-order: y = 1.84 − 0.012x | $k_1 = 0.012$ | 0.7163 |
| Pseudo-second-order: y = 0.22 + 0.0066x | $k_2 = 0.0002$, $q_e$=123.4 | 0.9559 |

## Adsorption Thermodynamics

The relationship of $q_e$ and $c_e$ at different temperatures is shown in Fig. 8. The $q_e$ value increased continuously with $c_e$ and the system temperatures, indicating the adsorption process was endothermic and driven by entropy (Mondal *et al.* 2011). The viscosity of the solution decreased with the increase of temperature, which facilitated the movement of metal ions across the outer boundary and diffusion onto the molecular chains of the adsorbent (Al-Qodah *et al.* 2000).
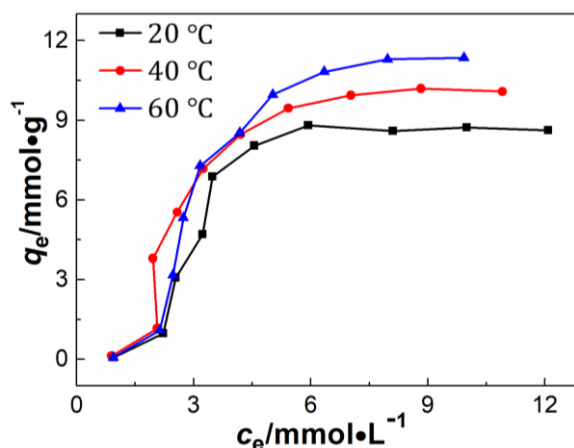


**Fig. 8.** Adsorption isotherms at different temperatures

The equilibrium adsorption isotherm is one of the most important methods for understanding the mechanism of adsorption. The Langmuir and Freundlich thermodynamic models are widely used to examine the thermodynamic data (Xie *et al.* 2014; Mona and Kaushik 2015). Therefore, the adsorption data of $SiO_2$/CPAM for Ca(II) were fitted with the Langmuir model (Tazrouti and Amrani 2009) and the Freundlich model (Freundlich and Helle 1939) as follows,

$$\frac{c_e}{q_e} = \frac{1}{bq_m} + \frac{c_e}{q_m}$$

(5)

$$\ln q_e = \ln K_F + 1/n \ln C_e$$

(6)

where $q_e$ (mg•g$^{-1}$) and $q_m$ (mg•g$^{-1}$) are the amount of Ca(II) adsorbed at equilibrium and the saturated adsorption capacity, respectively, $c_e$ (mg•L$^{-1}$) is the Ca(II) concentration at equilibrium, $b$ (L•mg$^{-1}$) is the Langmuir constant, and $K_F$ (mg•g$^{-1}$) and $n$ are the Freundlich constants related to the adsorption capacity and intensity, respectively.

The plots of $c_e/q_e$ *versus* $c_e$ and $\ln q_e$ *versus* $\ln C_e$ for Ca(II) adsorption are shown in Figs. 9 and 10. The values of $q_m$ and $b$ were calculated, respectively, according to the intercepts and slopes of the plots, as shown in Table 2. A linear relationship was observed

at different temperatures from Fig. 9, and $q_m$ values were 341.3 mg•g$^{-1}$, 432.9 mg•g$^{-1}$ and 526.3 mg•g$^{-1}$ at 20 °C, 40 °C, and 60 °C, respectively. Furthermore, the corresponding coefficients of determination ($R^2$) were all higher than 0.99, indicating that the adsorption of Ca(II) fitted well with the Langmuir isotherm at different temperatures. While the adsorption data were also fitted with the Freundlich model, all the $R^2$ values were less than 0.8 (Table 3).
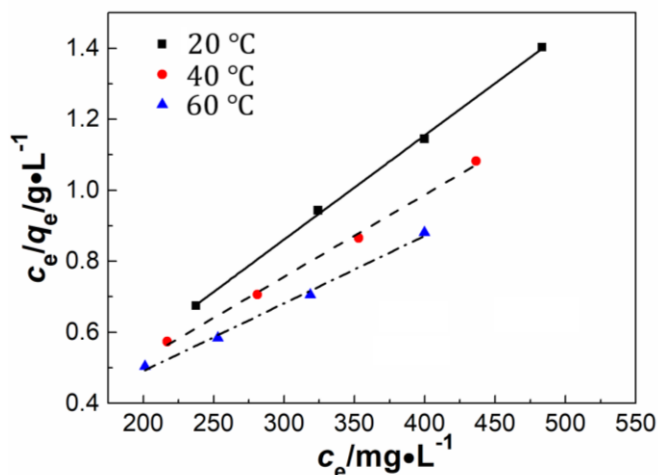


**Fig. 9.** Fitting of equilibrium data to the Langmuir isotherm model

**Table 2.** Regression Parameters of Langmuir Isotherm Model for Adsorption of SiO₂/CPAM for Ca(II)

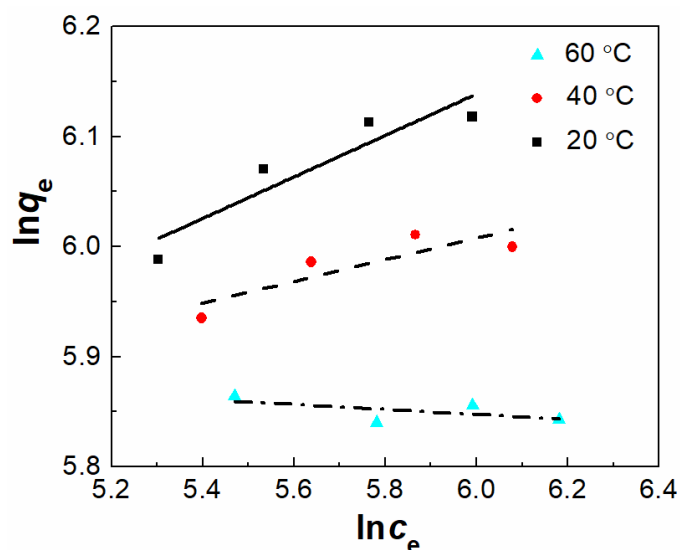| Temperature (°C) | Fitting Eq. | $q_m$ (mg•g$^{-1}$) | $b$ (L•mg$^{-1}$) | $R^2$ |
|---|---|---|---|---|
| 20 | y = 0.0029x – 0.019 | 341.3 | -0.15 | 0.9988 |
| 40 | y = 0.0023x + 0.063 | 432.9 | 0.037 | 0.9957 |
| 60 | y = 0.0019x + 0.11 | 526.3 | 0.017 | 0.9925 |



**Fig. 10.** Fitting of equilibrium data to the Freundlich isotherm model

Hence, the adsorption of the investigated metal ions on $SiO_2$/CPAM was monolayer and after saturation of this layer no further adsorption would take place (Alqadami *et al.* 2017), which matched the data of Fig. 8. In addition, the *b* value was higher than 0, indicating a spontaneous process; a larger *b* value indicated more stable products and an easier, stronger adsorption reaction (Chong and Volesky 1995). When the *b* value is lower than 0, that means the adsorbed product is unstable and easily desorbed (Li *et al.* 2011). The maximum *b* value was obtained at 40 °C, indicating that the adsorption was most favorable at this temperature.

**Table 3.** Regression Parameters of Freundlich Isotherm Model for Adsorption of $SiO_2$/CPAM for Ca(II)

| Temperature (°C) | Fitting Eq. | $K_F$ $(mg \cdot g^{-1})$ | $n$ | $R^2$ |
|---|---|---|---|---|
| 20 | y =5.98 – 0.022x | 0.98 | 0.17 | 0.05411 |
| 40 | y =5.40 + 0.098x | 243.14 | 11.80 | 0.4376 |
| 60 | y = 5.00 + 0.190x | 149.18 | 5.30 | 0.7982 |

**Analysis of Adsorption Mechanism**

The FT-IR spectra of $SiO_2$/CPAM before and after adsorbing Ca(II) (the latter is denoted as $SiO_2$/CPAM-Ca) were compared to make certain the adsorption mechanism, as illustrated in Fig. 2. The bands at 3352 $cm^{-1}$ and 3194 $cm^{-1}$ were attributed to asymmetrical and symmetrical stretching vibrations of N–H bonding in the primary amide groups in $SiO_2$/CPAM, and they were transferred to one strong and broad peak at 3397 $cm^{-1}$ with a shift towards the high band of 45 $cm^{-1}$ after adsorbing Ca(II). The peak at 1611 $cm^{-1}$ was ascribed to the stretching vibration of N-H bonding in $SiO_2$/CPAM and did not appear after adsorption, indicating that the N atoms in primary amines were involved in the chelation of Ca(II) (Deng and Chen 2003; Sun and Liang 2010). The adsorption peak of C=O bonding in amino groups in $SiO_2$/CPAM was moved from 1662 $cm^{-1}$ to 1668 $cm^{-1}$ (a shift of 6 $cm^{-1}$) because these two peaks in the amino group were overlapped with the acyloxy group.
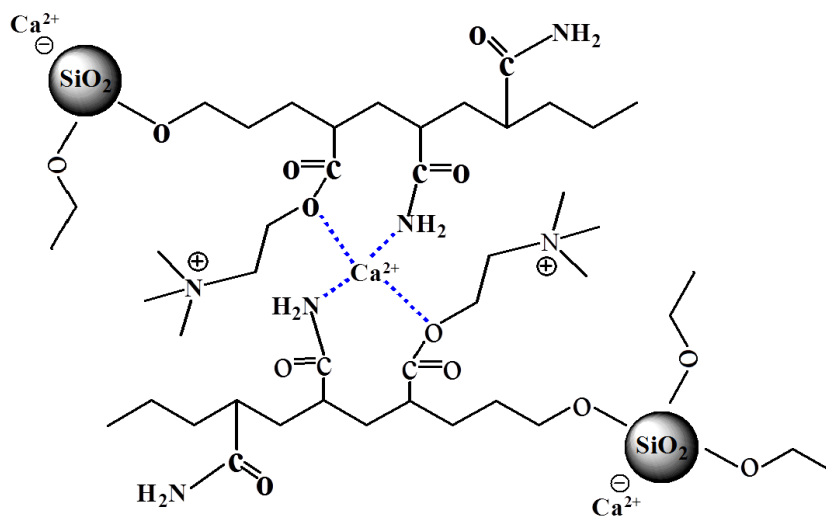


**Fig. 11.** Adsorption mechanism between $SiO_2$/CPAM and Ca(II)

The C=O bonding in amino groups cannot participate in chelation with metal ions, according to the reference (Deng and Chen 2003). Therefore, both the amino and acyloxy group were involved in the chelation reaction, resulting in the formation of p-$\pi$ coordination of Ca(II). It was also inferred that the adsorption of $SiO_2$/CPAM for Ca(II) was mainly based on chelation and electrostatic adsorption. The possible adsorption mechanism is presented in Fig. 11. The negative silicon hydroxyl group on the surface of $SiO_2$ interacted with positive Ca(II), and a large number of N and O atoms on the PAM molecular chain were chelated with Ca(II).

**Table 4.** Comparison of Adsorption Capacity ($Q_m$) of Ca(II) on Different Adsorbents

| Adsorbents | $Q_m$(mg•g$^{-1}$) | References |
|---|---|---|
| $SiO_2$/CPAM | 123.4 | This work |
| ACS | 32.0 | Ye *et al.* 2009 |
| P(AM-DMDAAC-AA) | 80.2 | Sun *et al.* 2012 |
| Poly(acrylate-acrylamide) Adsorbent Resin | 108.0 | Chen and Yu 2013 |

## Comparisons with Other Adsorbents

The maximum adsorption capacity ($Q_m$) of $SiO_2$/CPAM at 20 °C was compared with other adsorbents for the adsorption of Ca(II) (Table 4). All adsorbents exhibited a lower adsorption amount than that recorded in this work. Compared with the direct-chain molecule, more active adsorption sites occurred on the surface of dendritic $SiO_2$/CPAM, leading to chelation with Ca(II) easily. XPS data confirmed that AM residues were located on the molecular chain ends, while DAC residues were closer to the surface of $SiO_2$. Thus, $SiO_2$/CPAM was well-dispersed in solution, so that chelation with Ca(II) within the molecules grew easier and more stable and could not be influenced by the external force.

## CONCLUSIONS

1. The $SiO_2$/CPAM composites were successfully synthesized with a dendritic structure extending outward from the $SiO_2$ center.

2. High temperature was beneficial to the adsorption of Ca(II) onto $SiO_2$/CPAM due to the formation of chelation between Ca(II) and N and O atoms on the surface of $SiO_2$/CPAM. Adsorption of Ca(II) followed the Langmuir isothermal model well, as evidenced by a higher value of $R^2$. The kinetic data fitted well with the pseudo-second-order dynamic model.

3. The adsorption capacity was found to be superior to those of other reported adsorbents. The studies presented here reveal that it is a promising adsorbent to be applied for other contaminant metal ions in many fields.

## ACKNOWLEDGMENTS

## REFERENCES CITED

Alexander, M. R., Short, R. D., Jones, F. R., Michaeli, W., and Blomfield C.J. (1999). "A study of HMDSO/$O_2$ plasma deposits using a high-sensitivity and -energy resolution XPS instrument: Curve fitting of the Si 2p core level," *Applied Surface Science* 137(1-4), 179-183. DOI: 10.1016/S0169-4332(98)00479-6

Ali, S. M., Galal, A., Atta, N. F., and Shammakh, Y. (2017). "Toxic heavy metal ions removal from wastewater by nano-magnetite: Case study Nile river water," *Egyptian Journal of Chemistry* 60(4), 601-612. DOI: 10.21608/ejchem.2017.3583

Alqadami, A. A., Naushad, M., Abdalla, M. A., Ahamad, T., ALOthaman, Z. A., Alshehri, S. M., and Ghfar, A. A. (2017). "Efficient removal of toxic metal ions from wastewater using a recyclable nanocomposites: A study of adsorption parameters and interaction mechanism," *Journal of Cleaner Production* 156, 426-436. DOI: 10.1016/j.jclepro.2017.04.085

Al-Qodah Z. (2000). "Adsorption of dyes using shale oil ash," *Water Research* 34(17), 4295-4303. DOI: 10.1016/S0043-1354(00)00196-2

An, F. Q., Feng, X. Q., and Gao, B. J. (2009a). "Adsorption of aniline from aqueous solution using novel adsorbent PAM/$SiO_2$," *Chemical Engineering Journal* 151(1-3), 183-187. DOI: 10.1016/j.cej.2009.02.011

An, F. Q., Feng, X. Q., and Gao, B. J. (2009b). "Adsorption mechanism and property of a novel adsorption materials PAM/$SiO_2$ towards 2,4,6-trinitrotoluene," *Journal of Hazardous Materials* 168(1), 352-357. DOI: 10.1016/j.jhazmat.2009.02.042

Azizian, S. (2004). "Kinetic models of sorption: A theoretical analysis," *Journal of Colloid and Interface Science* 276(1), 47-52. DOI: 10.1016/j.jcis.2004.03.048

Ba, Y.-M., and Cao, Q.-S. (2014). "Comparative study on two calcium oxalate calculus models of rats," *Journal of Shanghai Jiaotong University Medical Science* 34(11), 1595-1598.

Bai, J.-R., Wang, Q., Qin, H., Zheng, G.-K., Yang, Y.-J., and Guan, X.-H. (2011). "Kinetics and thermodynamics of adsorption of heavy metal ions onto fly ash from oil shale," *Journal of Fuel Chemistry and Technology* 39(5), 378-384.

Chen, S., and Yu, X. (2013). "Softening property of polyacrylamide high adsorbent resin for hard water," *Journal of Wuhan Institute of Technology* 35(4), 39-42.

Chong, K. H., and Volesky, B. (1995). "Description of two-metal biosorption equilibria by Langmuir-type models," *Biotechnology and Bioengineering* 47(4), 451-460. DOI: 10.1002/bit.260470406

Clausen, D. N., Pires, I. M. R., and Tarley, C. R. T. (2014). "Improved selective cholesterol adsorption by molecularly imprinted poly(methacrylic acid)/silica (PMAA-$SiO_2$) hybrid material synthesized with different molar ratios," *Materials Science & Engineering: C* 44, 99-108. DOI: 10.1016/j.msec.2014.08.008

Deng, S. D., and Chen, J. P. (2003). "Aminated polyacrylonitrile fibers for lead and copper removal," *Langmuir* 19(12), 5058-5064. DOI: 10.1021/la034061x

Deng, T.-S., Zhang, Q.-F., Zhang, J.-Y., Shen, X., Zhu, K.-T., and Wu, J.-L. (2009). "One-step synthesis of highly monodisperse hybrid silica spheres in aqueous solution," *Journal of Colloid and Interface Science* 329(2), 292-299. DOI: 10.1016/j.jcis.2008.09.063

Elving, P. J., Meehan, E. J., and Kolthoff, I. M. (1987). "Treatise on analytical chemistry," *Journal of Pharmaceutical Sciences* 76(2), 186-187. DOI:10.1002/jps.2600760226

Fan, Q., Deng, H., and Wu, B. (2012). "Experimental study on the removal of calcium ions from water by modified waste molecular sieve," *Industrial Water Treatment* 32(6), 27-29.

Fielding, L. A., Tonnar, J., and Armes, S. P. (2011). "All-acrylic film-forming colloidal polymer/silica nanocomposite particles prepared by aqueous emulsion polymerization," *Langmuir* 27(17), 11129-11144. DOI: 10.1021/la202066n

Freundlich, I., and Helle, W. J. (1939). "Rubber die Adsorption in Lösungen," *J. Am. Chem. Soc.* 61, 2-28.

Gao, Y., Liu, Z., Guo R., and Wang, Y. (2009). "Synthesis of polyaspartic acid derivative and its characteristics in scale inhibition," *CIESC Journal* 60(8), 2107-2111.

Ghorai, S., Sinhamahpatra, A., Sarkar, A., Panda, A. B., and Pal, S. (2012). "Novel biodegradable nanocomposite based on XG-g-PAM/SiO$_2$: Application of an efficient adsorbent for Pb$^{2+}$ ions from aqueous solution," *Bioresource Technology* 119, 181-190. DOI: 10.1016/j.biortech.2012.05.063

Hadizade, G., Binaeian, E., and Emami, M. R. (2017). "Preparation and characterization of hexagonal mesoporous silica/polyacrylamide nanocomposite capsule (PAM-HMS) for dye removal from aqueous solutions," *Journal of Molecular Liquids* 238, 499-507. DOI: 10.1016/j.molliq.2017.05.026

Hettiarachchi, E., Kottegoda, N., and Perera, A. D. L. C. (2017). "Activated coconut coir for removal of water hardness," *Desalination and Water Treatment* 66, 103-110. DOI: 10.5004/dwt.2016.0339

Hemalatha, M., Butti, S. K., Velvizhi, G., and Mohan, S. V. (2017). "Microbial mediated desalination for ground water softening with simultaneous power generation," *Bioresource Technology* 242, 28-35. DOI: 10.1016/j.biortech.2017.05.020

Jedlicka, S. S., Rickus, J. L., and Zemlyanov, D. Y. (2007). "Surface analysis by X-ray photoelectron spectroscopy of sol-gel silica modified with covalently bound peptides," *Journal of Physical Chemistry B* 111(40), 11850-11857. DOI: 10.1021/jp0744230

Kong, Y., Wei, J., Wang, Z., Tao, S., Yao, C., and Chen, Z. (2011). "Heavy metals removal from solution by polyaniline/palygorskite composite," *Journal of Applied Polymer Science* 122(3), 2054-2059. DOI: 10.1002/app.34195

Li, Q., Jiang, P.-P., Lu, Y., and Zhang, D.-P. (2006). "Synthesis of cationic polymeric flocculant poly(DAC-AM) using inverse emulsion polymerization," *Journal of Southern Yangtze University (Natural Science Edition)* 5, 581-584.

Li, Q., Zhang, J., Xie, J., and Xu, W. (2011). "Performances and dynamics of substrate in constructed wetland system adsorbing phosphorus," *Technology of Water Treatment* 37(9), 64-67.

Li, S., Wei, Y., Kong, Y., Tao, Y., Yao C., and Zhou, R. (2015). "Electrochemical removal of lead ions using paper electrode of polyaniline/attapulgite composites," *Synthetic Metals* 199, 45-50. DOI: 10.1016/j.synthmet.2014.11.003

Li, Y., Ouyang, N., Lin, S., Ke, A., and Zhang, Q. (2012). "The sulfomethylated reaction of PAM/SiO$_2$ resins and adsorption of heavy metal ions," *New Chemical Materials*, 40(2), 95-97.

Mohanta, D., and Ahmaruzaman, M. (2018). "Bio-inspired adsorption of arsenite and fluoride from aqueous solutions using activated carbon@SnO$_2$ nanocomposites: Isotherms, kinetics, thermodynamics, cost estimation and regeneration studies," *Journal of Environmental Chemical Engineering* 6(1), 356-366. DOI: 10.1016/j.jece.2017.11.076

Mona, S., and Kaushik, A. (2015). "Chromium and cobalt sequestration using exopolysaccharides produced by freshwater cyanobacterium *Nostoc linckia,*" *Ecological Engineering* 82, 121-125. DOI: 10.1016/j.ecoleng.2015.04.037

Mondal, P., Roy, K., Bayen, S. P., and Chowdhury, P. (2011). "Synthesis of polypyrrole nanoparticles and its grafting with silica gel for selective binding of chromium(VI)," *Talanta* 83(5), 1482-1426. DOI: 10.1016/j.talanta.2010.11.037

Pan, T. (2015). *Spectral Analysis* (3rd Ed.), East China University of Science and Technology Press, Shanghai, China.

Peng, S., Zeng, Z., Zhao, W., Li, H., Chen, J., Han, J., and Wu, X. (2014). "Novel functional hybrid silica sol-gel coating for copper protection *via in situ* thiol-ene click reaction," *RSC Advances* (4), 15776-15781. DOI: 10.1039/c4ra00142g

Pirzada, T., Arvidson, S. A., Saquing, C. D., Shah, S. S., and Khan, S. A. (2012). "Hybrid silica-PVA nanofibers *via* sol-gel electrospinning," *Langmuir* 28(13), 5834-5844. DOI: 10.1021/la300049j

Pirzada, T., Arvidson, S. A., Saquing, C. D., Shah, S. S., and Khan, S. A. (2014). "Hybrid carbon silica nanofibers through sol-gel electrospinning," *Langmuir* 30(51), 15504-15513. DOI: 10.1021/la503290n

Saad, A., Bakas, I., Piquemal, J.-Y., Nowak, S., Abderrabba, M., and Chehimi, M. M. (2016). "Mesoporous silica/polyacrylamide composite: Preparation by UV-graft photopolymerization, characterization and use as Hg(II) adsorbent," *Applied Surface Science* 367, 181-189. DOI: 10.1016/j.apsusc.2016.01.134

Sun, L., and Liang, J. (2010). "Optimization of chelation of soybean peptides with calcium using response surface method," *Journal of the Chinese Cereals and Oils Association* 25(1), 22-27.

Sun, X., Dai, H., Wu, W.-B., Xu., M., and Qian, H.-W. (2012). "Synthesis of AM-DMDAAC-AA polyampholyte and its application as adsorbent of calcium ions in white water," *Transactions of China Pulp and Paper* 27(4), 18-22.

Sun, X., Dai, H., Qian, H.-W., Mao, S.-T., and Wang, J.-J. (2014). "Removal of Ca$^{2+}$ from papermaking whitewater by polyampholyte P(DMDAAC-AM-AA)," *Chemistry and Industry of Forest Products* 34(4), 51-58. DOI: 10.3969/j.issn.0253-2417.2014.04.009

Tazrouti, N., and Amrani, M. (2009). "Chromium (VI) adsorption onto activated kraft lignin produced from alfa grass (*Stipa tenacissima*)," *BioResources* 4(2), 740-755. DOI: 10.15376/biores.4.2.740-755

Wang, J., and Li, X. (2015). "Synthesis of polyacrylamide/modified silica composite hydrogels for synergistic complexation of heavy metal ions," *Desalination and Water Treatment* 53(1), 230-237. DOI: 10.1080/19443994.2013.837000

Wu, J.-Q., Ji, J.-F., Lin, Y.-D., and Zhu, H.-X. (2012). "Adsorption of copper ions by amino chelated bagasse cellulose in simulated heavy metals wastewater," *Transactions of China Pulp and Paper* 27(4), 23-27.

Xie, A., Ji, L., Luo, S., Wang, Z., Xu, Y., and Kong, Y. (2014). "Synthesis, characterization of poly(m-phenylenediamine)/palygorskite and its unusual and reactive adsorbability to chromium(VI)," *New Journal of Chemistry* 38(2), 777-783. DOI: 10.1039/c3nj01013a

Ye, C.-H., Dai, H., Wang, S.-M., Wang, Z.-L., and Yuan, G.-X. (2009). "Study on the ACS as adsorbent of calcium ions," *Transactions of China Pulp and Paper* 24(1), 85-90.

Zhao, G., Zhang, H., Fan, Q., Ren, X., Li, J., Chen, Y., and Wang, X. (2010). "Sorption of copper(II) onto super-adsorbent of bentonite-polyacrylamide composites," *Journal of Hazardous Materials*, 173(1-3), 661-668. DOI: 10.1016/j.jhazmat.2009.08.135